

## Supplementary Information

### Tailoring of mechanical properties of derivatized natural polyamino acids through tensile deformation

*Jessica R. May,<sup>a</sup> Cristina Gentilini,<sup>a</sup> David E. Clarke,<sup>a</sup> Yaroslav I. Odarchenko,<sup>b</sup> Denis V. Anokhin,<sup>c</sup> Dimitri A. Ivanov,<sup>\*b,c</sup> Kirill Feldman,<sup>d</sup> Paul Smith<sup>d</sup> and Molly M. Stevens<sup>a</sup>*

<sup>a</sup> *Departments of Materials and Bioengineering, Imperial College London, London, SW7 2AZ, U. K.*

<sup>b</sup> *Institut de Sciences des Matériaux de Mulhouse (CNRS UMR 7361), Université de Haute Alsace, 68057, France ; Tel : +333.89.60.88.07 ; E-mail: dimitri.ivanov@uha.fr*

<sup>c</sup> *Moscow State University, Faculty of Fundamental Physical and Chemical Engineering, 119991, Moscow, Russia*

<sup>d</sup> *Department of Materials, ETH Zürich, 8093 ,Switzerland*

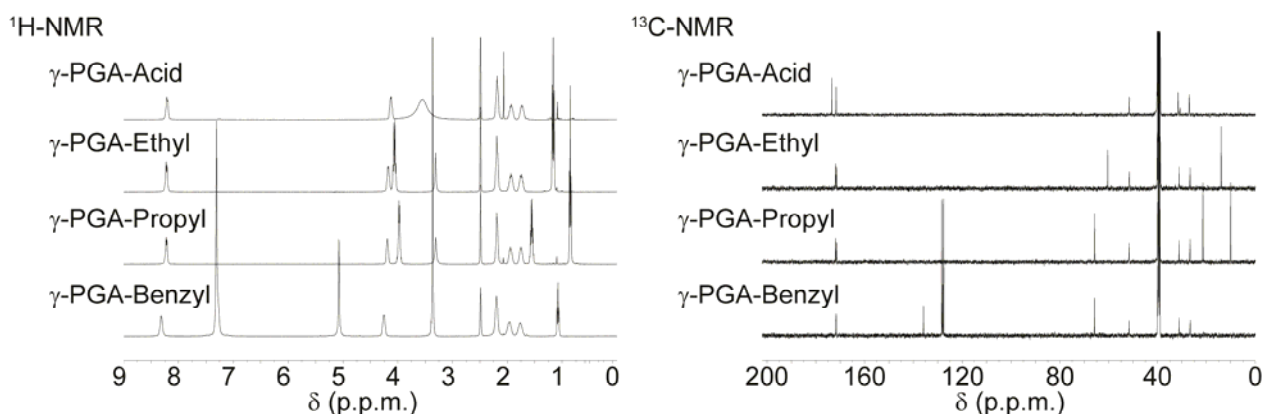


**Figure S1.**  $^1\text{H}$ - and  $^{13}\text{C}$ -NMR of  $\gamma$ -PGA-H and  $\gamma$ -PGA esters (in DMSO- $d_6$ ).

### *Polarised Optical Microscopy*

Polarized optical microscopy was employed to visualize the increase in macromolecular orientation in the drawn polymer samples. Figure S2 shows two tapes overlaid at  $\sim 90^\circ$  of  $\gamma$ -PGA-Bn, oriented to  $\lambda \geq 10$ , under cross-polarized light. Orientation was observed with a maximum light intensity at  $\pm 45^\circ$  to the polarizers, while no transmitted light was observed through the samples at  $0^\circ$ ,  $90^\circ$ , or the overlaid region of the two tapes, indicative of a high degree of uniaxial macromolecular order in the various tapes. Addition of a quarter wavelength retardation plate, displays both a subtractive (yellow) and additive (blue) effect through the highly oriented samples.

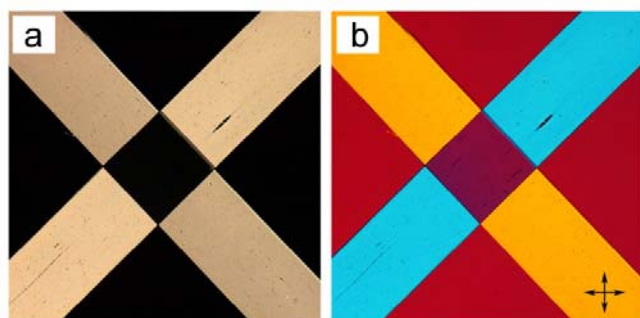


**Figure S2.** Representative polarized optical microscopy images of highly oriented  $\gamma$ -PGA-Bn polymer samples at maximum intensity, demonstrating the high macromolecular order causes a) two overlaid samples to act as polarizers to each other, b) further accentuated with addition of a first-order retardation plate.

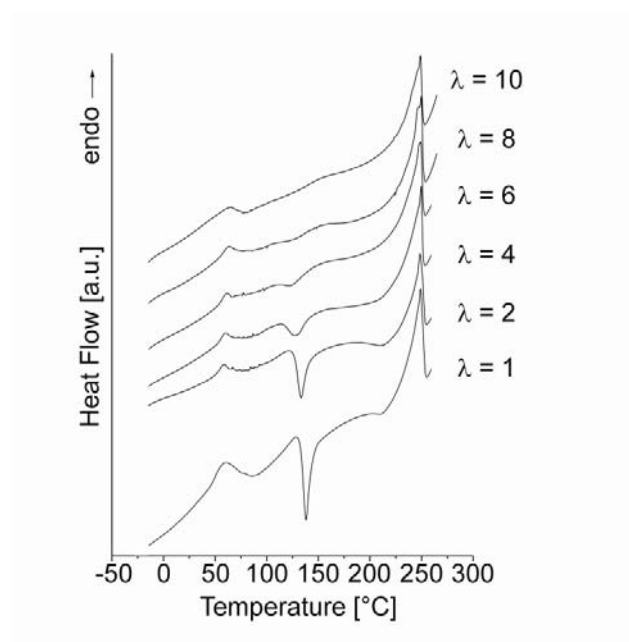


**Figure S3.** Representative first heating differential scanning calorimetry thermograms of  $\lambda$ -PGA-Et oriented to the draw ratios indicated, demonstrating an increase in degree of crystallinity of the material with increasing degree of orientation.

**Table S1.** Sources used to compile data for Fig. 4.

Human Tissue	Reference(s)
Articular Cartilage	[1-4]
Cornea	[5]
Cortical Bone	[4, 6]
Ligaments and Tendons	[4, 7-10]
Skin	[4]
Renal Capsule	[11]
Trabecular Bone	[6, 12]
Tracheal Cartilage	[13]

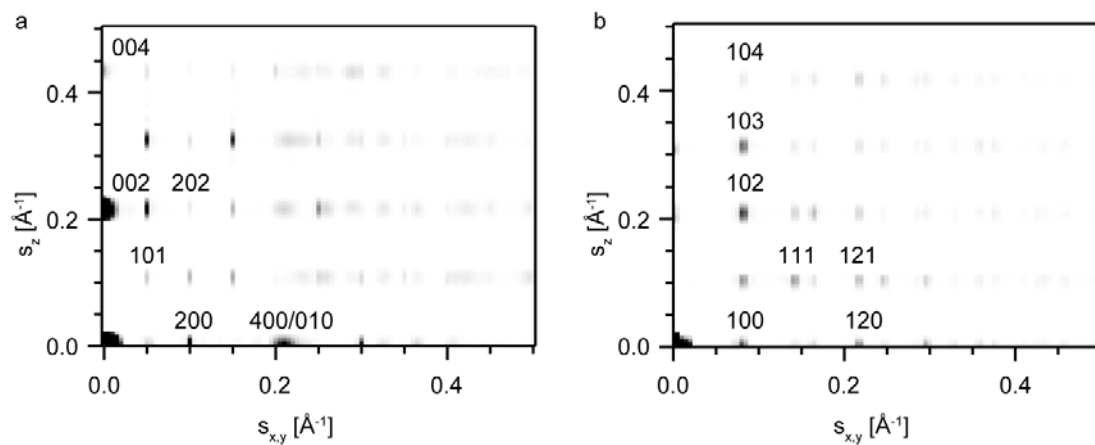


**Figure S4.** Simulated fiber X-ray patterns for a)  $\gamma$ -PGA-Pr and b)  $\gamma$ -PGA-Bn. The components of the  $s$ -vector along the  $x,y$  plane (equator) and  $z$ -axis (meridian) are comprised between 0 and  $0.5 \text{ \AA}^{-1}$ .

**Table S2.** Observed and calculated X-ray diffraction d-spacings corresponding to  $\gamma$ -PGA-Et,  $\gamma$ -PGA-Pr and  $\gamma$ -PGA-Bn.

$\gamma$ -PGA-Et				$\gamma$ -PGA-Pr				$\gamma$ -PGA-Bn				
layer line	hkl	$d_{\text{exp}}$ [Å]	$d_{\text{c}}$ [Å]	I	hkl	$d_{\text{exp}}$ [Å]	$d_{\text{c}}$ [Å]	I	hkl	$d_{\text{exp}}$ [Å]	$d_{\text{c}}$ [Å]	I
$l=0$	200	9.24	9.20	w	200	10.04	10.04	s	100	12.17	12.17	s
	010/400	4.61	4.55	vs	400	4.99	5.02	w	120	4.63	4.60	w
	210	3.76	4.08	w	010	4.69	4.76	vs		4.21	-	w
	600/510	2.89	3.07	vw	210	4.36	4.30	w				
	800	2.38	2.28	w	310	3.89	3.88	s				
					600	3.34	3.35	w				
					020	2.4	2.38	vw				
$l=1$	101	8.1	8.18	s	101	8.36	8.39	s	111	5.77	5.82	vw
	201	6.59	6.48	s	201	6.88	6.79	s	211	4.38	4.21	vw
	301	5.1	5.09	w	301	5.43	5.42	m				
	011/401	4.17	4.07	vs	011	4.22	4.23	vs				
	311/501	3.49	3.39	w	311	3.61	3.68	m				
	801	2.22	2.23	vw	701	2.73	2.74	vw				
$l=2$	002	4.55	4.57	w	002	4.66	4.62	m	102	4.73	4.78	s
	202	4.12	4.09	s	202	4.23	4.19	s	112	4.3	4.18	w
	302	3.67	3.66	w	302	3.79	3.80	s				
	412	2.7	2.64	vw	012	3.35	3.31	w				
					412	2.76	2.76	vw				
					612	2.36	2.35	vw				
$l=3$	303	2.72	2.73	vw	303	2.8	2.80	w	103	3.32	3.34	w
	403	2.58	2.54	vw	403	2.6	2.62	vw				
	503	2.37	2.35	vw	503	2.45	2.44	vw				

$l=4$	004	2.12	2.31	vw	104	2.54	2.54	vw
					204	2.36	2.39	vw

---

Lattice parameters

---

Orthorhombic; P2<sub>1</sub>22<sub>1</sub>;  
 for (h00) and (00l) h,l=2n  
 a=18.40Å, b=4.55Å,  
 c=9.13Å

Orthorhombic; P2<sub>1</sub>22<sub>1</sub>;  
 for (h00) and (00l) h,l=2n  
 a=20.07Å, b=4.76Å,  
 c=9.23Å

Hexagonal; P1  
 a=b=14.05Å,  
 c=10.40Å

---

### *X-ray pattern simulation*

The simulated X-ray patterns were computed with home-built routines written in Igor Pro (Wavemetrics Ltd.). The computation of the scattering intensity  $I(\mathbf{s})$  for each point of the reciprocal space  $\mathbf{s}$  was performed according to:

$$I(\mathbf{s}) = \left| \sum_{n=0}^N f_n(|\mathbf{s}|) e^{-2\pi i \mathbf{s} \cdot \mathbf{r}_n} \right|^2$$

where  $N$  is the total number of atoms in the unit cell (hydrogens were omitted from the calculation for simplicity) and  $\mathbf{r}_n$  are the absolute coordinates of the  $n$ -th atom. The atomic scattering factors  $f_n(\mathbf{s})$  for each value of the norm of the scattering vector  $|\mathbf{s}|$  were calculated by interpolating the tabulated values.<sup>14</sup> The two-dimensional X-ray pattern of a uniaxially oriented sample was calculated as following:

$$I_f(s_{xy}, s_z) = \sum_{\varphi=0}^{2\pi} I(s_{xy} \cos \varphi, s_{xy} \sin \varphi, s_z)$$

where  $s_{xy} = \sqrt{s_x^2 + s_y^2}$ .

The simulated fiber X-ray patterns for  $\gamma$ -PGA-Pr (a) and  $\gamma$ -PGA-Bn (b) polymers presented in Figure S4 are in reasonable agreement with the experimental patterns. Thus for experimental and simulated diffractograms of  $\gamma$ -PGA-Pr the strongest equatorial peak (i.e. 010) corresponds to the distance between the hydrogen-bonded sheets. The simulated intensity of the meridional 002 and 004 peaks is characterized by a similar intensity ratio. In the case of  $\gamma$ -PGA-Bn the two strong experimental equatorial peaks with indices 100 and 120 are also visible on the calculated 2D pattern. The presence of

strong 102 and 103 peaks is also in agreement with the experimental diffractogram. As was found in the experiment, the well-pronounced meridional reflections are absent from the simulated pattern, which proves the 5/2 helical backbone conformation of  $\gamma$ -PGA-Bn.

### *Polarized Raman spectroscopy*

Raman measurements were carried out on a confocal Raman microspectrometer Labram-BX 40. The 632.81nm excitation polarized light from a HeNe laser light source was focused through a 50x/0.95 objective (Olympus; Japan) onto flat oriented fibers fixed in a specially designed holder to eliminate the signal from the substrate. The laser power was 5 mW. The device calibration was done using Si peak at  $520\text{cm}^{-1}$ . A single spectrum resulted after integration of 50 measurements.

The polarized Raman spectra of oriented  $\gamma$ -PGA-Et (a) and  $\gamma$ -PGA-Pr (b) films are presented in Figure S5. The characteristic Raman peaks at 3295 (Amide A,  $\nu$  N-H), 1740 (ester group,  $\nu$  C=O) and  $1642\text{ cm}^{-1}$  (Amide I,  $\nu$  C=O) show perpendicular dichroism for both polymers. This situation is expected for a structure with C=O and N-H bonds oriented normal to the chain axis. Thus the Raman data generally confirms the proposed structural model.

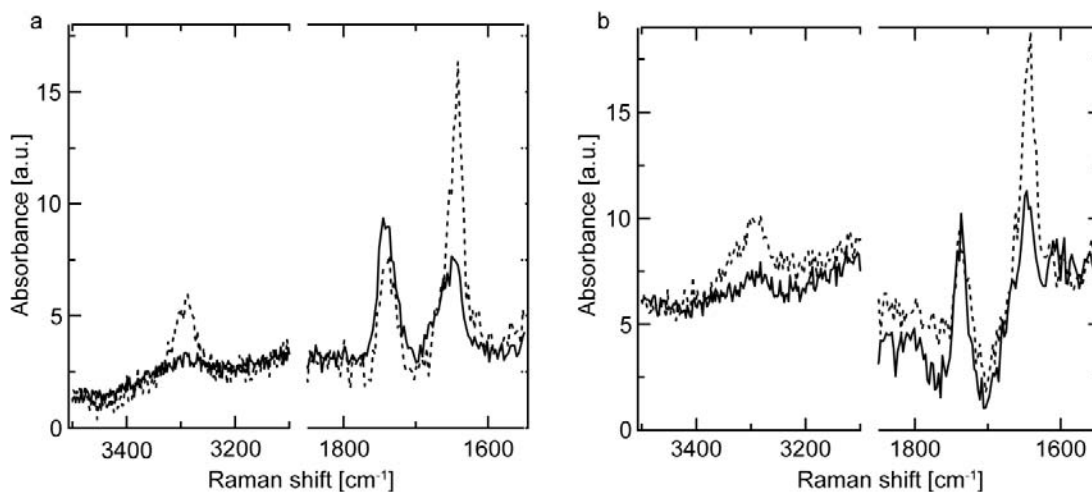


**Figure S5.** Polarized Raman spectra corresponding to oriented films of a)  $\gamma$ -PGA-Et and b)  $\gamma$ -PGA-Pr. The solid and dotted lines denote the parallel and perpendicular orientation of the film stretching direction with respect to the polarizer.

### *References*

1. Kempson, G. E.; Muir, H.; Pollard, C.; Tuke, M. *Biochimica Et Biophysica Acta* **1973**, *297*, 456-472.
2. Kuo, Y. C.; Hsu, Y. R. *Journal of Biomedical Materials Research Part A* **2009**, *91A*, 277-287.
3. Moutos, F. T.; Freed, L. E.; Guilak, F. *Nature Materials* **2007**, *6*, 162-167.
4. Reis, R. L.; San Román, J., *Biodegradable systems in tissue engineering and regenerative medicine*. CRC Press: Boca Raton, 2005.
5. Zeng, Y. J.; Yang, J.; Huang, K.; Lee, Z. H.; Lee, X. Y. *Journal of Biomechanics* **2001**, *34*, 533-537.
6. Webster, T. J., *Nanotechnology for the regeneration of hard and soft tissues*. World Scientific: Hackensack, N.J.; Singapore, 2007.
7. Ethier, C. R.; Simmons, C. A., *Introductory biomechanics : from cells to organisms*. Cambridge University Press: Cambridge; New York, 2007.
8. Neumann, P.; Keller, T. S.; Ekstrom, L.; Perry, L.; Hansson, T. H.; Spengler, D. M. *Journal of Biomechanics* **1992**, *25*, 1185-1194.
9. Majima, T.; Funakosi, T.; Iwasaki, N.; Yamane, S. T.; Harada, K.; Nonaka, S.; Minami, A.; Nishimura, S. I. *Journal of Orthopaedic Science* **2005**, *10*, 302-307.
10. Quapp, K. M.; Weiss, J. A. *Journal of Biomechanical Engineering-Transactions of the Asme* **1998**, *120*, 757-763.
11. Snedeker, J. G.; Niederer, P.; Schmidlin, F. R.; Farshad, M.; Demetropoulos, C. K.; Lee, J. B.; Yang, K. H. *Journal of Biomechanics* **2005**, *38*, 1011-1021.
12. Gil, F. J.; Sevilla, P.; Aparicio, C.; Planell, J. A. *Journal of Alloys and Compounds* **2007**, *439*, 67-73.

13. Roberts, C. R.; Rains, J. K.; Pare, P. D.; Walker, D. C.; Wiggs, B.; Bert, J. L. *Journal of Biomechanics* **1998**, *31*, 81-86.

14. Wilson, A. J. C.; Prince, E.; International Union of Crystallography., *International tables for crystallography. Vol. C, Mathematical, physical and chemical tables*. 2d ed.; Published for the International Union of Crystallography by Kluwer Academic Publishers: Dordrecht; Boston, 1999.